International Geology Review, 2014
http://dx.doi.org/10.1080/00206814.2014.951977

Unearthing earthquakes and their tsunamis using multiple proxies: the 22 June 1932 event and a probable fourteenth-century predecessor on the Pacific coast of Mexico

María-Teresa Ramírez-Herrera[a,b]*, Néstor Corona[c], Marcelo Lagos[d], Jan Černý[e,f], Avto Goguitchaichvili[g], James Goff[h], Catherine Chagué-Goff[h,i], Maria Luisa Machain[j], Atun Zawadzki[i], Geraldine Jacobsen[i], Arturo Carranza-Edwards[i], Socorro Lozano[k] and Lindsey Blecher[h]

[a]*Departamento de Geografía Física, Instituto de Geografía, Universidad Nacional Autónoma de México, Ciudad Universitaria, DF, Mexico;* [b]*Laboratorio Universitario de Geofísica Ambiental, Universidad Nacional Autómoma De México – Campus Morelia, Michoacán, México;* [c]*Centro de Estudios en Geografía Humana, El Colegio de Michoacán, La Piedad, Michoacán, México;* [d]*Laboratorio de Investigación de Tsunamis, Instituto de Geografía, Pontificia Universidad Católica de Chile, Santiago, Chile;* [e]*Department of Geological Sciences, Faculty of Science, Masaryk University, Brno, Czech Republic;* [f]*Institute of Geology, Academy of Sciences of the Czech Republic, Praha-Lysolaje, Czech Republic;* [g]*Laboratorio Interinstitucional De Magnetismo Natural, Instituto De Geofisica, Universidad Nacional Auomoma De Mexico – Campus Morelia, Michoacán, México;* [h]*School of Biological, Earth and Environmental Sciences, University of New South Wales, Sydney, NSW, Australia;* [i]*Australian Nuclear and Science Technology Organisation, Kirrawee, NSW, Australia;* [j]*Instituto de Ciencias del Mar y Limnología, Universidad Nacional Autónoma de México, Ciudad Universitaria, DF, Mexico;* [k]*Instituto de Geología, Universidad Nacional Autónoma de México, Ciudad Universitaria, DF, Mexico*

(*Received 21 March 2014; accepted 2 August 2014*)

Tsunami deposits have been widely studied in temperate latitudes, but the intrinsic difficulties associated with tropical coastal environments, and the intensity of bioturbation in these habitats, limit the possibilities of analysing these formations. Here, we investigate the deposits on the Colima coast of Mexico, which overlies the subducting Rivera and Cocos Plates, in order to reconstruct the tsunami inundation history and related hazard. We developed a multi-proxy study aimed to recognize and date historical and palaeotsunami deposits, including historical data on the effects of a known tsunami, geomorphological mapping, stratigraphic, grain size, organic matter content, diatoms, geochemical composition, magnetic susceptibility, and anisotropy of magnetic susceptibility, together with radiometric dating (^{210}Pb and ^{14}C). We identified two probable tsunami deposits at Palo Verde estuary including a historical event associated with the Mw 6.9 earthquake on 22 June 1932 and a palaeotsunami most likely generated by a similar event in the fourteenth century. This work shows that it is possible to identify both historical and palaeotsunamis in the tropical environment of Mexico's Pacific coast. These data will serve to enhance our understanding of tsunami deposits in tropical environments and of the regional tsunami hazard.

Keywords: tsunami deposits; palaeotsunami; tropical environment; multi-proxy approach; Pacific coast; México

1. Introduction

The human and economic losses produced by the most recent tsunamis of the Indian Ocean 2004, Chile 2010, and Japan 2011 show the need to understand better this natural phenomenon. During the past decades, studies based on geological evidence became an important tool for determining the prehistoric occurrence of large and great earthquakes and tsunamis (e.g. pioneering work by Atwater and Moore 1992; Atwater and Hemphill-Halley, 1996; Hutchinson *et al.* 1997; Pinegina and Bourgeois 2001; Nanayama *et al.* 2003; Atwater *et al.* 2005; Cisternas *et al.* 2005; Nelson *et al.* 2006; Baker *et al.* 2013; and others). In recent years, our ability to identify the impact of prehistoric tsunamis in the geological record has been greatly improved through the analysis of historical deposits such as the 2004 Indian Ocean tsunami (e.g. Liu *et al.* 2005; Moore *et al.* 2005; Szczucinski *et al.* 2006; Hawkes *et al.* 2007; Paris *et al.* 2007, 2010; Jankaew *et al.* 2008; Monecke *et al.* 2008; Sawai *et al.* 2009; Goto *et al.* 2012a; and others), the 2006 Java tsunami (e.g. Moore *et al.* 2011), and the 2011 Tohoku-oki tsunami (e.g. Goto *et al.* 2011, 2012b, 2014; Szczucinski *et al.*, 2012; and many others). Despite these advances, it is still difficult to distinguish between prehistoric tsunami deposits and those laid down by other possible high-energy inundation events, such as storm surges (e.g. Tuttle *et al.* 2004; Morton *et al.* 2007), even more in tropical coastal areas where physical and chemical weathering can be rapid, and bioturbation may be intense (e.g. Kamatani 1982; Kench *et al.* 2006, 2008; Jankaew *et al.* 2008). A few studies show a wide variety of proxies that must be used to achieve such goals (Kortekaas and Dawson 2007; Ramirez-Herrera *et al.*, 2007; Goff *et al.* 2010a, 2012a; Chagué-Goff *et al.* 2012b). The use of multiple proxies may all prove useful, when analysed together, in determining the origin of anomalous sediment deposits in coastal areas (e.g. Ramirez-Herrera *et al.* 2007; Goff *et al.*

*Corresponding author. Email: tramirez@igg.unam.mx

2010a; Chagué-Goff *et al.* 2011, 2012, 2012a, 2012b; Font *et al.* 2013).

The Pacific coast of Mexico, parallel to the Mexican subduction zone, is an area where little scientific survey work has been undertaken in the immediate aftermath of tsunami or storm surge inundation. Even for reasonably recent events, the extent and depth of inundation may only be estimated from anecdotal evidence (Cumming 1933; Abe *et al.* 1986; Sanchez and Farreras 1993; Valdivia *et al.* 2012; NGDC 2013), and their stratigraphic signatures have been investigated in only a few studies (Ramirez-Herrera *et al.*, 2005, 2007, 2009, 2012). The principal source of tsunamis along the Pacific coast of Mexico is the plate boundary between the Rivera-Cocos plates and the North America plate (Figure 1). The locked zone at this plate interface ruptured in two stages in June 1932. A Ms = 8.2 earthquake on 3 June and its aftershocks of 18 June (Ms = 7.8) were followed by another large (Ms = 6.9) aftershock on 22 June (Singh *et al.* 1981; Astiz and Kanamori 1984, 1985). Both ruptures triggered tsunamis that caused local flooding. A lower magnitude event, the 22 June earthquake, produced a larger tsunami with a reported run-up 11 m high in Cuyutlán, Colima, Mexico (Sánchez and Farreras 1993; Corona and Ramírez-Herrera 2012a, 2012b).

This study aims to identify the deposits of a historical tsunami, namely the 1932 tsunami, and prehistorical events, using multiple proxies in a area where the preservation of geologic evidence might be poor due the intrinsic characteristics of the tropics and the frequent storms (hurricanes) on the Pacific coast of Mexico. While there are photographs, newspaper reports, and eyewitness accounts of the 1932 tsunami and the resulting damage at the time, finding the tangible evidence in the geologic record is an important part of assessing the long-term hazard of tsunamis on the Mexican–Pacific coast. We also believe it is crucial to identify and differentiate tsunami deposits from storm deposits for a coast frequently hit by storms. Finding predecessors of the 1932 event is a first step forward to building a palaeotsunami record of the Mexican Pacific coast. An initial survey of low-lying areas along the central western coast of Mexico, in Colima, revealed a site with anomalous sand beds within fine-grained sedimentary sequences. We present here lines of evidence from the Palo Verde (PV) estuary to determine whether these anomalous sand beds were laid down by tsunamis and to distinguish them from storm deposits.

1.2. *History of tsunamis*

The Cuyutlán coast has a record of six tsunamis: 3, 18, 22, and 29 June 1932; 19 September 1985; and 9 October 1995 (Sánchez and Farreras 1993). However, based on the

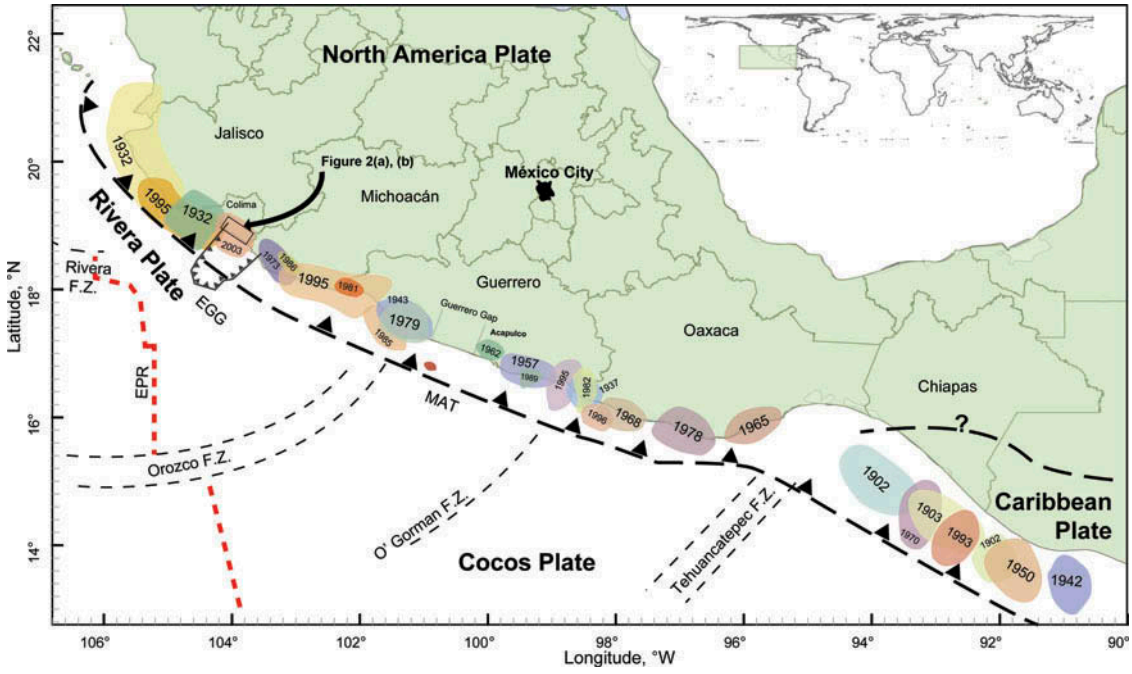

Figure 1. Tectonic and seismic setting of the Pacific coast of Mexico: MAT, Middle US Trench; FZ, fracture zones; EPR, East Pacific rise; EGG, El Gordo Graben. Shaded circles indicate rupture areas and years of most important subduction seismic events since the beginning of the last century. Small black dashed lines indicate fracture zones; the thick black dashed line with arrowheads shows the subduction zone. The thick red dashed line shows the location of the EPR. The Caribbean Plate boundary is shown with dashed lines and a question mark where it is not well-defined. Plate convergence rates are shown in cm year^{-1}. Arrowheads indicate the direction of convergence. Dashed square shows the location of Figure 2a, b (not to scale).

interpretation of historical data (HTDB/WLD 2013; NGDC (National Geophysical Data Center – National Oceanic and Atmospheric Administration) 2013), it was inferred that at least 27 tsunamis had probably affected the Cuyutlán coast between 1875 and 2011. Historical data also indicate that an earlier tsunami inundated the salinas (salt pans) of San Pantaleon (currently El Real town), located 14 km southeast of PV estuary, and penetrated about 400 m inland on 13 November 1816 (Oseguera-Velázquez 1967).

A reconstruction of the 22 June tsunami through historical and ethnographic analysis allowed us to determine that the sea level was higher than normal at the time of inundation due to coastal subsidence produced by the 3 June earthquake; the sea also receded before the tsunami inundated the Cuyutlán coast (Corona and Ramirez-Herrera, 2012a, 2012b). Inundation heights were estimated to be up to 11 m, as estimated from photographs with an error of ±10 cm. The tsunami inundated an area 450–2000 m inland within 2–3 min, with the inland extent of tsunami inundation varying depending upon the local topography and taking about 3 h to drain out (Chagué-Goff *et al.* 2012a, 2012a, 2012b). Modelling reported in Corona and Ramirez-Herrera (2012a) was based on four well-identified control points, and a continuous map of the distribution of inundation levels was constructed based on the selection of the best fit equation (Chagué-Goff *et al.* 2012a). The 22 June tsunami characteristics fit a VIII tsunami intensity level (Papadopoulos and Imamura 2001).

2. Tectonic setting and site description

Seismic activity along the Pacific coast of Mexico is mostly attributable to subduction of the Rivera and Cocos plates beneath the North America plate (Figure 1). Unlocking of this plate interface typically produces Mw 7.3–8.2 earthquakes (NGDC (National Geophysical Data Center – National Oceanic and Atmospheric Administration) 2013), with an average recurrence interval of about 80 years (Singh *et al.* 1985), but larger Mw > 8.5, although less common, have occurred here, such as the approximately Mw 8.6 earthquake on 28 March 1787 (Suarez and Albini 2009; NGDC (National Geophysical Data Center – National Oceanic and Atmospheric Administration) 2013). The largest earthquake of the last century resulted from the rupture of the Rivera plate interface on 3 June 1932 (Ms 8.2). This was followed by aftershocks on 18 June (Ms 7.8) and 22 June (Ms 6.9) (Singh *et al.* 1981; Astiz and Kanamori 1984, 1985, 1998; HTDB/WLD (Historical Tsunami Database for the World Ocean) 2013; NGDC (National Geophysical Data Center – National Oceanic and Atmospheric Administration) 2013). In October 1995, a Mw 7.8 earthquake occurred in this region. However, no great earthquakes (Mw > 8) have occurred along the Rivera–North America plate interface since 1932 (Figure 1).

The 22 June 1932 event generated an unusually large tsunami (run-up height approximately 11 m) for its seismic magnitude (Cumming 1933). This event devastated the town of Cuyutlán and also caused damage in other locations (Chagué-Goff *et al.* 2012a, 2012b). The source for this unusually large tsunami has been interpreted as a 'tsunami earthquake', i.e. a slow rupture event (Okal and Borrero 2011), although others suggest that it was caused by a submarine slump (Cumming 1933; Corona and Ramírez-Herrera 2012a). The 22 June tsunami affected 75 km of the coast of Colima, between 19.06° N and 104.31° W near Manzanillo Bay and 18.68° N and 103.74° W near Boca de Apiza (NGDC (National Geophysical Data Center – National Oceanic and Atmospheric Administration) 2013). Most of the damage occurred along a segment about 6 km long on the Cuyutlán coast (Figure 2a).

The Jalisco-Colima coastal area is at risk from tsunamis generated by the Mexican subduction zone. We therefore selected this region, an approximately 115 km-long coastal stretch, to search for geological evidence of historical tsunami deposits. The PV estuary, near Cuyutlán in Colima, was identified as a key area because a post-tsunami survey was completed there after the 1932 earthquake, identifying sites of inundation and run-up (Figure 2a) (Cumming 1933; Corona and Ramírez-Herrera 2012a). Furthermore, the local geomorphology is favourable for the preservation and study of the geological signatures of past tsunamis (e.g. marshes and an estuary and back-barrier lagoon) (Figure 2a, b, c). Anthropogenic land-use changes after 1932 (e.g. coconut cultivation, new infrastructure, and buildings) complicated the geomorphologic interpretation of tsunami effects. Nevertheless, it is possible to interpret and identify some morphologic features (Goff *et al.* 2009) caused by the 1932 tsunami. Tsunami-scour fans associated with the overwash flow were identified close to the current main street in Cuyutlán. Broken dune features formed by tsunami erosion were found in several segments of the beach ridges that parallel the shoreline. Likewise, probable remnant pedestals were also located in the estuary at a distance of 400–850 m from the shoreline, behind the PV site (Figure 2b, d) (Corona and Ramírez-Herrera 2012a).

The adjacent PV area (Figure 2b) is a microtidal estuary exposed to moderate wave action from predominantly SSW winds (in summer) and SW winds (in winter). The estuary lies behind a 34 km-long, 275 m-wide beach and sand-barrier capped by sand dunes ranging up to about 7.5 m above sea level (masl) near the study site (Figure 2c). A coastal plain extends inland to the back-barrier lagoon with the Laguna de Cuyutlán bordered on all side by fringes of mangrove swamps. Saltpans (salinas) extend to the northwest of Cuyutlán lagoon. The PV study site is situated east of the Cuyutlán lagoon, behind the aeolian deposits of the coastal plain and close to the mangrove

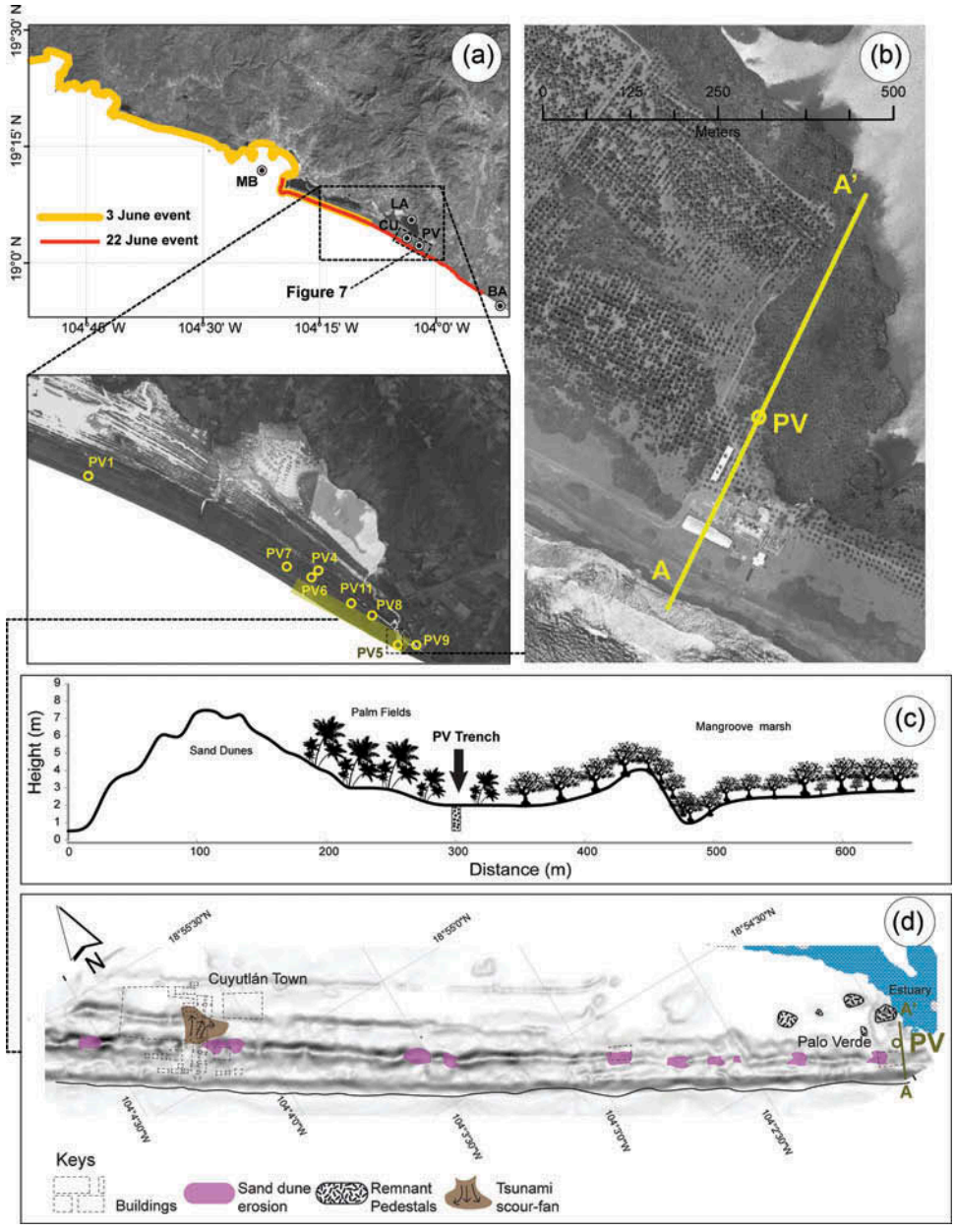

Figure 2. Location map of the Palo Verde (PV) estuary. (a) Laguna Cuyutlán (LA) and beach sand back-barrier on the Colima coast. Dashed square shows the location of Figure 7. Yellow and red lines show inundated areas along the Jalisco and Colima coast based on historical reconstruction and modelling of the 3 June and 22 June tsunamis, respectively. CU, Cuyutlán; MB, Manzanillo Bay; ER, El Real; BA, Boca de Apiza. The inset shows the location of test pits. (b) Close-up to the Palo Verde estuary, the yellow line indicates the surveyed topographic profile. (c) Topographic profile, the box shows the study site and Palo Verde trench (Figure 3) location. (d) Map of geomorphic features produced by a tsunami. SPOT and WorldView 2 images.

marshes. The estuary connects with the sea seasonally: the mouth closes during the winter dry season and opens during the summer rainy season. Relative sea-level elevation data are not available for the nearest coastal area; however, data from elsewhere along the Pacific Coast indicate that sea level stabilized between ~6000 and 5200 years ago (Curray *et al.* 1969; Atwater *et al.* 1977; Sirkin 1985; Ortlieb 1986; Voorhies 2004; Caballero *et al.* 2005). Thus, the Cuyutlán brackish lagoon barrier probably formed by high-energy marine deposition after sea level stabilized, by ca. 6000 cal BP. Based on data from other lagoons on the west coast of Mexico, beach barrier construction was concluded at least by 4630 BP (Ramirez–Herrera *et al.*, 2005, 2007). Currently, soils of the area are derived from local granite, while to the north of the site, intermediate extrusive igneous rocks

(andesites) dominate the local geology (Lancin and Carranza 1976).

3. Materials and methods

No single analytical technique will unequivocally identify buried tsunami deposits. We applied a combination of techniques (historical/ethnographic, geomorphological, stratigraphic, grain size, loss on ignition, diatom, foraminifera, ostracods, geochemical, magnetic susceptibility, and anisotropy of magnetic susceptibility [AMS]), ^{210}Pb and ^{14}C dating, analyses, and modelling. Some of these techniques were described by Ramirez-Herrera *et al.* (2012).

We used satellite images (Google Earth) and aerial photographs (1: 75,000) to identify relatively undisturbed sites in areas known to have been impacted by the 22 June 1932 historic tsunami (Cumming 1933). We focused on areas with high preservation potential (e.g. wetlands, swales between beach ridges, marshes, and estuaries) for sediment coring and trenching. After a detailed field exploration and extraction of 42 hang-auger cores and test pits in the area in 2009, we found that most explored pits and cores did not display continuous sand units, and in many cases, sand was exposed in patches or was removed by crabs. We therefore selected the site that showed continuous sand units and was most likely beyond the storm-wave influence, at least 150–200 m from the present shoreline (Figure 2a, b). This site is located by the PV estuary where the estuary banks showed the greatest potential for detailed study. Also the sedimentary record of the PV estuary appeared relatively undisturbed as opposed to the swales and marshes of the Cuyutlán town and the Cuyutlán lagoon, which have been disturbed by construction and salt extraction activities, respectively, and bioturbation (Chagué-Goff *et al.* 2012a). The trench (PV) is located in a depression 275.3 m inland at an elevation of 2.0 masl and is separated from the ocean by sand dunes with a maximum height of 7.5 masl (Figure 2c) (18°53′ 55.52″ N, 104°2′1.60″ W). Sampling was performed in the field, *in situ* in the trench, and was mainly through the collection of an entire section ('monoliths') of trench wall using a 100 cm-long section of guttering driven horizontally into the sediment and a PVC pipe 80 cm long by sledge hammer. All samples were stored at the laboratory for further analysis, and lengths were adjusted for compaction. We focused our study and analyses on one monolith, one PVC 80 cm long and cubes for magnetic property analyses, the results of which are reported here.

Storm and tsunami deposits are generated by similar depositional mechanisms, making their discrimination hard to establish using classic sedimentologic methods alone. We therefore applied a complementary technique, together with other proxies, to help identify tsunami-induced deposits using rock and environmental magnetism. This method was tested by other authors (Cuven *et al.* 2013; Font *et al.* 2010; Wassmer *et al.* 2010) and also tested locally (Ramírez-Herrera *et al.* 2012; Goguitchaichvili *et al.*, 2013). It appears to be a promising additional tool to be used in conjunction with other proxies to aid in identifying tsunami-induced deposits. Samples for magnetic analysis (magnetic susceptibility and AMS) adopted the collection technique described by Ramírez-Herrera *et al.* (2012) and Goguitchaichvili, *et al.* (2013). Low-frequency magnetic susceptibility measurements were carried out using AGICO Kappabridge MFK1-B equipment. To obtain the susceptibility (k) measurements at high and low frequency (k hf at 4700 Hz, k lf at 470 Hz), we used a Bartington MS2B apparatus. Mass-specific susceptibility (κ) was calculated using these k values. Equally, frequency-dependent susceptibility k FD [%] = (k lf – k hf) × 100/k lf was used to determine the possible presence of superparamagnetic (SP) grains in the magnetic fraction (Dearing 1994; Dearing *et al.* 1996; Heller *et al.* 1993; Maher *et al.* 1994). AMS in low field was measured at room temperature using a Kappabridge KLY-2 device. The measured values $K1$, $K2$, and $K3$ correspond to maximum, intermediate, and minimum susceptibility, respectively. Based on these principal directions of magnetic susceptibility, the shape parameter $T = 2 \ln (K2/K3)/\ln (K1/K3) - 1$ (Jelínek 1981), the degree of anisotropy $P = K1/K3$ (Nagata 1961), mean magnetic susceptibility $K_m = (K1 + K2 + K3)/3$, and corrected anisotropy degree P_j (Jelinek 1981) were calculated. Measured data were processed using Anisoft 4.1 software.

In this study, we searched for pollen and ostracods in samples in order to complement the diatoms and foraminifer microfossil record of palaeoenvironments. We performed petrographic analysis following Carranza-Edwards *et al.* (2009) and particle size analysis to determine textural parameters (Folk 1974) on beach samples collected at the intertidal beach zone and at the beach berm at the study site, in order to infer the source of sands in the PV estuary trench. To obtain the chronology of the younger sediments, we used the ^{210}Pb dating method (Appleby 2001). Samples were analysed at the ANSTO Institute for Environmental Research by alpha spectrometry following methods described in Harrison *et al.* (2003). Eight samples from the PV core between 0 and 19 cm were dried and ground up. Each sample was spiked with polonium-209 (^{209}Po) and barium-133 (^{133}Ba) tracers. Each sediment sample was subsequently leached with hot concentrated acids to release polonium and radium. Polonium was autoplated onto silver disks after adding the reducing agent hydroxylammonium chloride. Radium and barium were isolated by co-precipitation and collected as colloidal micro-precipitates on fine-membrane filter papers. The activities of ^{210}Po on the silver disks and ^{226}Ra on the membrane filters were determined by alpha spectrometry. Each membrane filter was also counted by gamma

spectrometry to measure the ^{133}Ba tracer activity. Chemical yield recoveries of ^{210}Po and ^{226}Ra were calculated using the recoveries of ^{209}Po and ^{133}Ba tracers, respectively. The unsupported ^{210}Pb activity on each sediment sample was calculated by subtracting the ^{226}Ra activity from the ^{210}Po activity. Unsupported ^{210}Pb activities from the samples are plotted against depth. For chronological control of older samples, five samples were taken from the trench at PV and radiocarbon dated at ANSTO. The sandy sediments were treated to remove carbonates and humic acids; the remaining carbon was processed through to graphite, which was measured using accelerator mass spectrometry (2MV HVEE Tandem) as described in Fink *et al.* (2004). The results were corrected for fractionation using δ^{13}C values obtained using a separate elemental analysis – isotope ratio mass spectrometry determination of the graphite targets used for AMS measurements. Where graphite sizes were too small, an estimated δ^{13}C value was used. Final ^{14}C ages were calculated following Stuiver and Polach (1977). Age calibration was done using the OxCal 4.2 calibration program with the IntCal13 data-set (Reimer *et al.* 2013).

4. Results

4.1. Geological signature

4.1.1. Stratigraphy

The base of the PV L-shaped trench (16 m × 8 m and 91.5 cm deep) terminates below the water table. It consists of five distinct units, of which three are sand beds at 10–32 cm, 45.5–77 cm, and 77–91.5 cm depth (Figures 3 and 4). The blue-grey sand layer, 'PV1', at 10–32 cm depth has a sharp basal contact, uneven along the trench, and contains pebbles and rip-up clasts (Figure 3, Photo 1, Photo 3, and Photo 4) of the underlying bioturbated orange-brown clayey silt (32–45.5 cm depth). The second sand unit, PV2, between 45.5 and 77 cm below the ground surface has a sharp basal contact and pebbles up to 12 mm in diameter near the base with

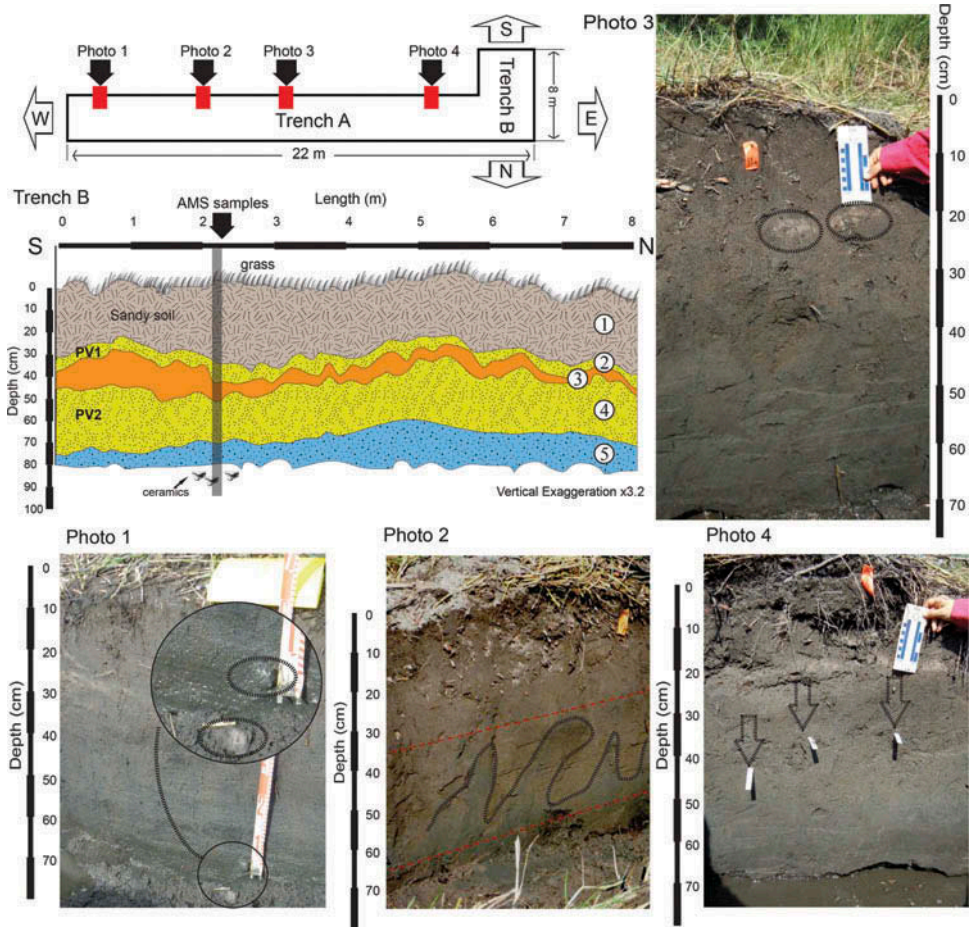

Figure 3. Palo Verde trench: Top inset shows orientation, shape, and length of PV trench; trench log of face B shows trench stratigraphy. PV1 and PV2 indicate position of two sand units; (Photo 1) circles indicate pebbles, (Photo 2) flame structures, (Photo 3) black dotted ovals outline rip-up clasts, (Photo 4) detail of pebbles scattered through PV2 unit.

several scattered throughout the PV2 unit (Figure 3, Photo 4). This unit contains flame structures of material injected from the underlying unit, suggesting liquefaction (Figure 3, Photo 2). The lowest unit is a blue silty-clayish sand at 77–91.5 cm depth. Unfortunately, water table partly covered this unit and its basal contact; thus samples collected for further analyses on this unit were not complete to study in its entirety (Figure 3, Photo 4).

4.1.2 *Particle size*

Changes in mean grain size are evident between the sand beds and finer sediments. A thin (1 cm) unit separates the upper sandy soil (0–10 cm depth) and the underlying grey sand (10–32 cm depth) (Figure 4). This 22 cm-thick sand unit (PV1) is normally graded, consisting of medium sand at the top with scattered pebbles (approximately 5 mm) near the base (Figure 4a). Due to the low percentage of pebbles (~2%), these were not included in grain size calculations (Figure 4a), although the fining upwards is illustrated in the stratigraphy. A marked grain size contrast is observed with the underlying clayey-silt unit (32–45.5 cm depth). The second sand unit (PV2) at 45.5–77 cm depth is normally graded, as is the lowest sand unit at 77–91.5 cm depth. The cumulative grain size analysis shows significant changes in the sand percentage, with 88–97.1% sand in the PV1 sand compared with 4.2–68.2% in the underlying clayey-silt unit (32–45.5 cm depth). Sorting is highly variable, ranging from moderately to well sorted in the sandy soil (0–10 cm depth) and

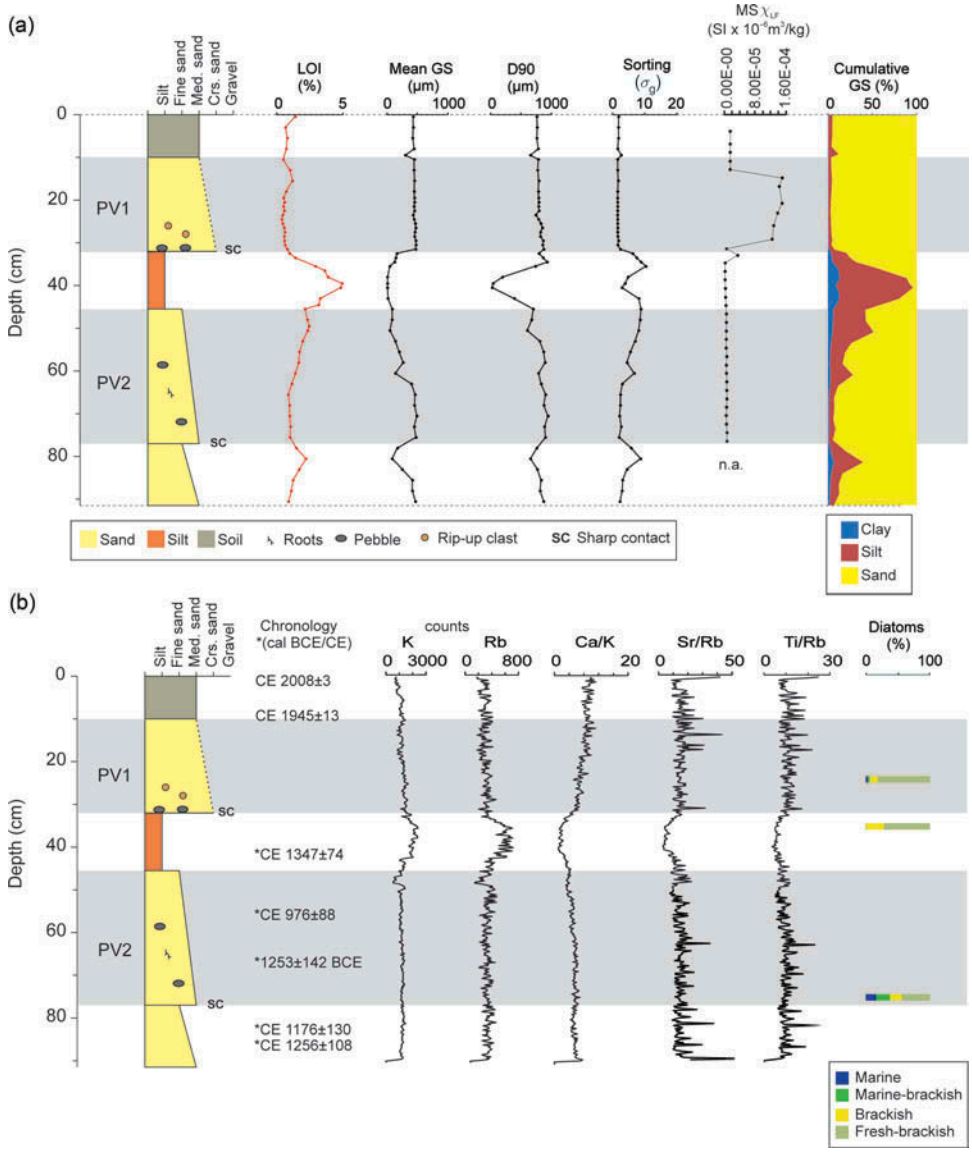

Figure 4. Palo Verde trench: (a) stratigraphy, ^{210}Pb and ^{14}C dates (refer to Tables 1 and 2 for details), LOI, mean grain size (GS), sorting, magnetic susceptibility, and cumulative GS; (b) stratigraphy, LOI, selected geochemical ratios, and diatoms. PV1, sand unit 1; PV2, sand unit 2.

grey sand (10–32 cm depth) and very poorly sorted in the clayey-silt unit (32–45.5 cm) (Figure 4a). PV2 is poorly sorted at the base to very poorly sorted towards the top. A similar pattern is apparent in the lower silty-clayish sand unit at 77–91.5 cm depth.

4.1.3. *Organic content and geochemistry*

PV1 and PV2 sand units are characterized by a low organic content (loss on ignition – LOI) of 0.5 to <2.5% (there is only 2.0% LOI in the upper sandy soil; 0–10 cm depth). The clayey-silt unit interbedded between PV1 and PV2 on the other hand contains more organic matter, with LOI ranging between 1 and 4.9 % (Figure 4a). Elemental distribution appears to be strongly controlled by lithology. Rubidium (Rb) and potassium (K) concentrations are lower in the sandy units than in the finer clayey-silt unit, reflecting the lower clay content in the coarser units (Figure 4b) (e.g. Chagué-Goff 2010). Thus K and/or Rb were used to normalize or correct for the grain size effect. The Ca/K, Sr/Rb, and Ti/Rb ratios are higher in the sandy units (Figure 4b).

4.1.4. *Magnetic properties*

The magnetic susceptibility profile is low throughout the entire sequence, 0–77.5 cm, with the exception of PV1, which has high values from 13 to 30 cm depth (Figure 4a). AMS results show that the minimum susceptibility direction (**K3**) is almost parallel with the pole of the horizontal bedding, while the mean direction of maximum susceptibility (**K1**) is 105° azimuth, although **K1** is more scattered, in comparison with **K3** (Figure 5a). Three distinct clusters are evident when comparing the degree of anisotropy (P) against mean magnetic susceptibility (K_m), with the K_m value differing by an order of magnitude between the red cluster and the others (Figure 5b). The majority of samples have an oblate AMS with T values between 0 and 1, although one notable exception (Figure 5c, green square) has a markedly higher degree of anisotropy (P). This sample represents the clayey-silt unit, and it has a higher corrected degree of anisotropy P_j (Figure 6, green circle).

The PV stratigraphic profile reflects a combination of four different magnetic fabrics (Figure 6). Samples from AMS Unit I incorporate the sand soil from 0 to 10 cm and possess almost no preferred *K1* orientation. In AMS Unit II, which is essentially representative of PV1, there is a preferred orientation of 116° azimuth, with one outlier (yellow square) at 43° azimuth. This latter sample was collected near the base of PV1. AMS Unit III represents the clayey-silt unit (32–45.5 cm) underlying PV1 and is characterized by a scattered *K1* orientation. Unit IV is from PV2 and has a stronger preferred orientation of 96° azimuth.

4.1.5. *Foraminifera, ostracods, and diatoms*

No foraminifers, ostracods, or pollen were recorded in any of the samples from the PV trench. The absence of foraminifers and ostracods could be due to the nature of the deposits (sandy) that precluded the preservation of their calcitic carapaces, while the absence of pollen in the samples also could be related to the general particle size of the profile. Sands are the dominant particles, and because most pollen grains are between 20 and 30 μm preservation is generally poor. This might also be due to either a lack of suitable pollen-producing plants or poor preservation potential (Yawsangratt *et al.* 2012). However, three analysed samples from the PV trench produced a useful number of diatom frustules. At 24–25 cm depth in PV1, there are marine and marine-brackish taxa (3.4% polyhalobous, 3% mesohalobous) such as *Diploneis smithii* and *Paralia sulcata* (Figure 4b). The clayey-silt unit at 35–36 cm depth is dominated by freshwater taxa (oligohalobion indifferent = 71.6%); however, at 75–76 cm depth in PV2, there are abundant marine and marine-brackish taxa (16.6% polyhalobous, 21.6% mesohalobous) including *Cyclotella meneghiniana*.

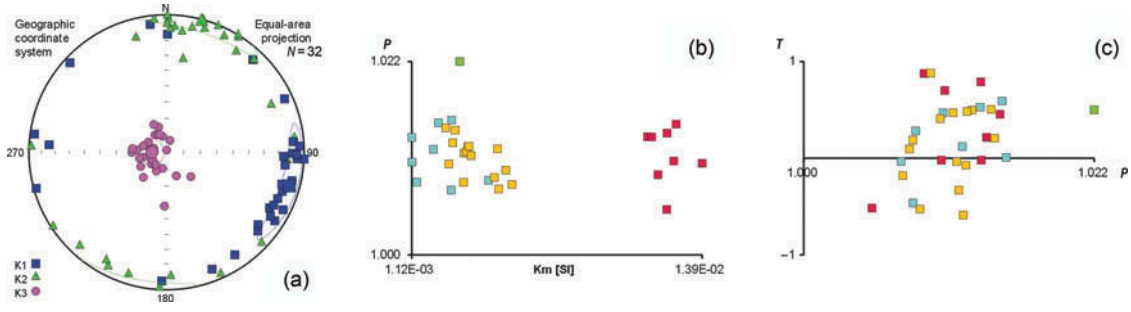

Figure 5. Palaeomagnetism of Palo Verde samples. (a) Principal directions of AMS plotted as a lower hemisphere equal-area projection. **K1, K2,** and **K3** represents maximum, intermediate, and minimum susceptibility directions, respectively. (b) Degree of anisotropy (P) *versus* bulk mean magnetic susceptibility (K_m). (c) Jelinek's shape parameter (T) *versus* degree of anisotropy (P). Red, light blue, and yellow squares correspond to Unit II, Unit III, and Unit IV, respectively. The green square corresponds to the uppermost sample in the PV2 horizon. Unit I was excluded due to the small number of samples taken.

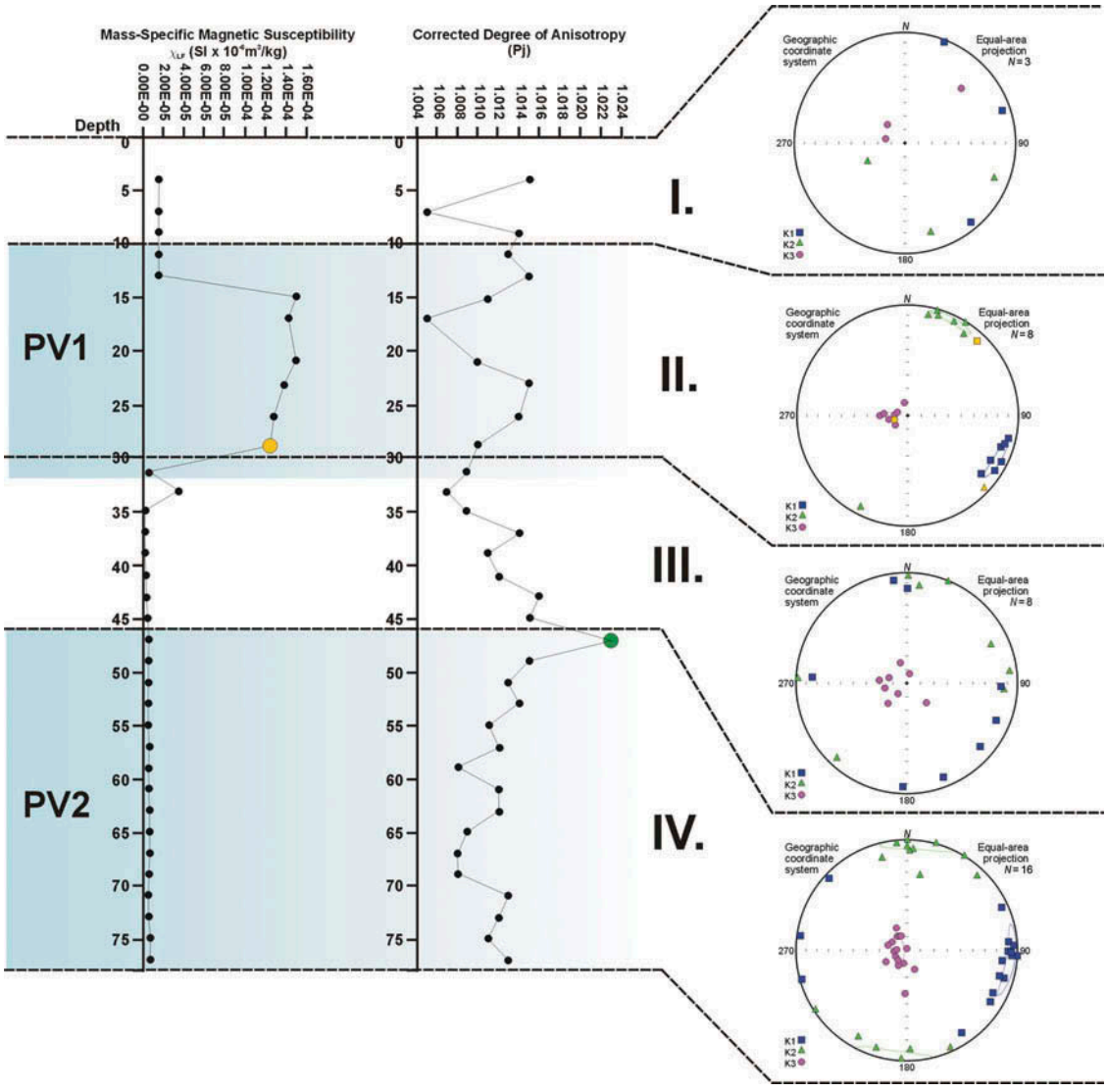

Figure 6. Magnetic susceptibility *versus* depth in relation to four different magnetic fabrics. The yellow-coloured samples represent marked changes in maximal susceptibility direction of the lower part of the PV1 horizon. The green circle represents the highest value of corrected degree of anisotropy parameter (P_j). It corresponds with the uppermost sample of the PV2 horizon. **K1, K2,** and **K3** represent maximum, intermediate, and minimum susceptibility directions, respectively. Principal directions of AMS are plotted as a lower hemisphere equal-area projection.

4.1.6. *Petrology*

Results from petrographic analysis and particle size from beach samples collected at the intertidal beach zone and at the beach berm at the study site indicate that sands (Supplementary Document 4: Table 4; see http://dx.doi.org/10.1080/00206814.2014.951977) from the beach berm and intertidal beach zone are richer in heavy minerals (HMs). This beach is directly exposed to the constant offshore wave action that controls the presence of medium sands, moderately well sorted, symmetrical, and leptokurtic (Supplementary Document 4: Table 4). These sands are rich in volcanic rock fragments that cause an excess of supra-crustal lithics (volcanic and sedimentary) over sands derived from deep-sited rocks (plutonic and metamorphic) due to the most abundant outcrops of volcanic rocks in the Armeria River basin, located southeast of the PV estuary, and transported to the northwest by the longshore current.

4.1.7. *^{210}Pb and radiocarbon age*

Unsupported ^{210}Pb activity was determined by alpha spectrometry. ^{210}Pb activity was low (12.1 ± 0.7 Bq/kg at 0–1 cm depth) largely because of the coarse-grained sediment (3.3–5.0% mud, 0.1–0.4% clay). As such, the derived dates are reasonably tentative (Table 1). The unsupported ^{210}Pb profile decays down the section to

Table 1. ^{210}Pb CIC and CRS data for the Palo Verde trench.

ANSTO ID	Depth (cm)	Total ^{210}Pb (from ^{210}Po activity) (Bq/kg)	Supported ^{210}Pb (from ^{226}Ra activity) (Bq/kg)	Unsupported ^{210}Pb (Bq/kg)	Calculated CIC ages (years)	Calculated CRS ages (years)
N611	0.0–1.0	14.4 ± 0.7	2.3 ± 0.2	12.1 ± 0.7	3 ± 3	4 ± 2
N612	2.5–3.5	8.1 ± 0.4	3.0 ± 0.3	5.1 ± 0.5	19 ± 5	21 ± 5
N613	5.0–6.0	7.9 ± 0.4	3.5 ± 0.3	4.4 ± 0.5	35 ± 7	39 ± 6
N614	7.5–8.5	7.0 ± 0.3	3.4 ± 0.4	3.6 ± 0.5	51 ± 10	69 ± 11
N615	10.0–11.0	6.4 ± 0.3	5.2 ± 0.5	1.2 ± 0.6	67 ± 13	133 ± 34
N616	12.5–13.5	7.5 ± 0.4	2.8 ± 0.3	4.7 ± 0.5		
N617	15.0–16.0	8.6 ± 0.4	3.1 ± 0.3	5.5 ± 0.5		
N618	17.5–18.5	5.8 ± 0.3	4.1 ± 0.4	1.7 ± 0.5		

11 cm depth, but the activities increase at 12.5–13.5 cm and 15–16 cm depth. This apparent inconsistency may be related to the transition from the sandy soil (0–10 cm depth) up to the sand unit PV1 (10–32 cm depth, see Figure 4). While the former sandy soil was most probably formed *in situ*, the material for the underlying sand of PV1 seems likely to have been sourced elsewhere.

Sediment ages were determined using the CIC (constant initial concentration) and CRS (constant rate of supply) ^{210}Pb dating models using unsupported ^{210}Pb data between 0 and 11 cm depth only (see Supplementary Document 1: Figure 1). At 10–11 cm depth, the CIC model estimated an age of 67 years (1945 ± 13 year CE), whereas the CRS model estimated an age 133 ± 34 years (Table 1). There is a strong historical record of a tsunami in 1932 at 10–11 cm depth; therefore, the calculated CIC model ages are likely to be more reliable than the CRS model for this core.

Results of radiocarbon dating (Table 2) reflect the relative paucity of datable organic material which limited the number of samples that could be analysed. The samples which were dated had very low levels of carbon after pre-treatment, giving bulk organic carbon yields that ranged between 0.091% and 0.002%. It is recognized that radiocarbon ages from bulk organic materials do not give accurate ages as the sources of the carbon cannot be identified and may be from multiple sources of different ages (Walker *et al.* 2007). Given the very small sample sizes, and that the material is of unknown origin, the ^{14}C ages obtained here should not be considered absolute ages, but may provide approximate ages. A plot of the calibrated age ranges (see Supplementary Document 2: Figure 2) shows that samples from within the lowest sand unit (83.5–85 and 86–87.5 cm depth) have overlapping calendar date ranges (CDRs) ca. 1250 CE. The clayey-silt on the other hand has a slightly younger calendar date of ca. 1350 CE at 41–41.25 cm depth, although all three dates overlap between 1256 ± 108 and 1347 ± 74 CE and may be contemporaneous. These two units bracket the sand unit PV2, indicating that it probably dates to around 1300 CE (1256–1347 CE), although two radiocarbon samples (at 56–57.5 and 66–67.7 cm depth) taken from PV2 unit produced CDRs of 976 ± 88 CE and 1253 ± 142 BCE, respectively, are considerably older than the bracketing sediments.

5. Discussion

The multi-proxy approach adopted in the study has been applied to a series of sand layers in the tropical environment of PV. We argue that two of the sand layers identified at PV are likely to be tsunami deposits, one at 10–32 cm depth (PV1) and the other at 45.5–77 cm depth (PV2).

Table 2. Radiocarbon ages on bulk organic material in sediments.

Lab code	Depth (cm)	δ ^{13}C (‰)	^{14}C Age ± 1σ (year BP)	Calibrated age (2σ range with probability) (cal BP)	Calibrated age (2σ range) (cal BCE/CE)	Mean age ± 2σ (cal BCE/CE)
OZP322	41–42.5	−17.0 ± 0.1	620 ± 50	540–667 (95.4%)	AD 1284–1410	AD 1347 ± 74
OZP323	56–57.5	−25.0*	1055 ± 40	920–10,578 (95.4%)	AD 893–1029	AD 976 ± 88
OZP324	66–67.5	−25.0*	3010 ± 40	3072–3273 (79.7%)	1386–1129 BC	1253 ± 142 BC
				3285–3341 (15.7%)		
OZP326	83.5–85	−25.0*	840 ± 60	675–834 (17.6%)	AD 1045–1107	AD 1176 ± 130
				834–909 (77.8%)	AD 1177–1276	
OZP325	86–87.5	−23.0 ± 0.2	750 ± 60	561–597 (7.4%)	AD 1160–1316	AD 1256 ± 108
				633–792 (88.0%)	AD 1354–1389	

Notes: Radiocarbon ages were calibrated using OxCal v4.2 (Bronk Ramsey 2009) using the IntCal13 calibration data-set (Reimer *et al.* 2013).
*δ^{13}C value is assumed.

The probable tsunamigenic origin of PV1 is supported by a number of proxies. First, this is a fining upward unit with a sharp basal contact, both typical traits of tsunami deposits. The higher magnetic susceptibility in this unit suggests a marked change in detrital input (Rothwell *et al.* 2006; Font *et al.* 2010; Ramírez-Herrera *et al.* 2012, 2013; Goguitchaichvili *et al.* 2013). Furthermore, the inclusion of clay intraclasts (rip-ups) is considered to be indicative of significant erosion of the underlying substrate with subsequent entrainment associated with a high-energy inundation event. In this instance, the deposit has been laid down at a site at least 270 m from the coast behind a 7 m-high sand barrier. Diatom frustules preserved within this unit include a large proportion of taxa with an affinity for high salinity levels, while marine species are absent from the underlying clayey-silt layer which has only brackish to brackish-fresh species, indicating that this sediment most likely comes from the sea. Geochemical data, however, do not show clear evidence of salinity. This is mostly likely attributed to the LOI associated with coarse sediment, which impedes the preservation of salinity indicators, such as Cl and S (Chagué-Goff *et al.* 2002; Chagué-Goff 2010, 2012a). However, Ca/K and Sr/K data reflect either the occurrence of shell hash (e.g. Rothwell *et al.* 2006; Chagué-Goff 2010) or a different mineralogical assemblage from an external source in the sandy layers. The higher Ti/Rb ratio is most likely to reflect the occurrence of heavy minerals (such as rutile). Heavy minerals are often found in tsunami deposits and interpreted as evidence of high-energy conditions (Chagué-Goff 2010), although it is recognized that they occur in a wide range of settings, including beach, fluvial, alluvial, colluvial, and aeolian environments (Dill 2007).

PV2 is also a fining upward sand unit with flame structures at its base, the latest suggesting liquefaction, a low LOI (increasing upwards), and abundant marine diatoms near the base. Magnetic susceptibility values are lower throughout this unit. When compared with PV1, the evidence for a high-energy marine inundation is equally strong, and on balance this therefore appears to be a precursor of the 1932 event.

PV1 reflects a significant increase of mass-specific magnetic susceptibility unlike studies carried out in different tectonic settings (e.g. Font *et al.* 2010, 2013). At our study site, the sources of iron oxides are volcanic rocks (intermediate to basic), widely spread around the area, and from volcanoes (in particular the Colima volcano and Volcan del Fuego) along this active continental margin of Mexican Pacific Coast. Here, beach sands are enriched with iron oxides (Carranza-Edwards *et al.* 2009), and also petrographic data of the beach berm and intertidal beach zone from the study site show an enrichment of heavy minerals, and this is the source of a positive magnetic anomaly. In the case of PV2, there is also a slight positive change in magnetic susceptibility (Figure 5). We hypothesize that this smaller positive change in magnetic susceptibility might be explained by either: (1) post-depositional biological activity; however AMS and MS alone cannot solve this problem; (2) the lower magnetic susceptibility anomaly in case of PV2 could be caused by the deposition of better sorted sediment. Two times higher density of magnetite (5.17 g/cm^3) in comparison with other sediment particles such as quartz (2.65 g/cm^3) definitely affects deposition. For example, coastal dune sand could be better sorted by aeolian processes, and it could have lower content of heavy minerals than the other beach features. Perhaps, PV2 sediment is a relic of destroyed beach dune by a tsunami? Or maybe the current which deposited PV2 has better sorting capability, because of lower energy, in comparison with the current which deposited PV1? The coast of Colima near PV estuary, as stated before, shows coastal sand dunes that could explain the source of sand of PV2 and the lower magnetic susceptibility of this deposit.

Recent AMS studies in tsunami investigations presented possible ways of studying magnetic fabrics by using AMS parameters plotted against the depth (e.g. Wassmer *et al.* 2010; Cuven *et al.* 2013; Schneider *et al.* 2014). In the case of PV, just P and P_j parameters displayed significant change at 46–48 cm depth (Figures 5 and 6). The other parameters displayed random patterns rather than significant changes in the PV profile. On the other hand, the bulk mean magnetic susceptibility (Figure 5b) and mass-specific magnetic susceptibility (Figure 6) displayed changes along the complete profile.

As expected, some changes in the stratigraphy are observed, since tsunami deposits are laid down in a different hydrodynamic regime to the other layers. In the past, it has been shown that different AMS fabrics are related to different hydrodynamic regimes (Taira 1989; Tarling and Hrouda 1993) and transport directions of sediments (e.g. Rees and Woodall 1975; Ellwood and Ledbetter 1977); therefore, several different AMS fabrics should be expected along one vertical profile, which is composed of several layers.

In this study, we attempted to separate AMS fabrics and to show how the differences between fabrics can be reflected along all the profile. The separation was done by a combination of: (1) selecting clusters of samples based on the maximal susceptibility direction (**K1**) changes; (2) selecting samples based on clustering in Jelinek's diagram comparing P *versus* K_m (Figure 5b); (3) the stratigraphy; and (4) the sequential depth of samples was taken also into account.

Separation of Unit I and Unit II was mainly based on changes in maximal susceptibility direction **K1** (Figure 6). If we consider stratigraphy, the change in AMS fabric fits better than significant change of mass-specific magnetic susceptibility (Figure 6). In this case however, the separation of Unit I could be hypothetical because of a small

number of samples which represent this unit. Separation of Unit II and Unit III is based on a significant change in mean bulk magnetic susceptibility (Figure 5b) and mass-specific magnetic susceptibility (Figure 6). Separation of Unit III and Unit IV is based on a slight change in mean magnetic susceptibility of the clusters in Jelinek's diagram comparing the degree of anisotropy (P) against mean magnetic susceptibility (K_m) where two clusters overlap (Figure 5b, yellow and light blue squares). This rough distinction showed two different AMS magnetic fabrics. After that, the exact distinction of clusters was correlated with stratigraphy and the sequential depth of samples. Although **K1** direction in equal-area projection was no longer scattered from 44 cm depth and preferred orientation appeared, the limit between Unit III and Unit IV was established in 46 cm above the sample, which represents a remarkable increase of P (Figure 5b, green square) as well as P_j parameters (Figure 6, green circle).

Four magnetic fabrics are associated with different stratigraphic units. Fabrics from the upper and middle soils (overlying PV1 and PV2, respectively) can be interpreted as sedimentary fabrics from a low-energy sedimentary environment with no marked magnetic orientation imparted by currents and where **K1** direction is scattered (Tarling and Hrouda 1993). In comparison, the fabrics from PV1 and PV2 are interpreted as those that have been significantly influenced by currents flowing in ESE–WNW (116° azimuth) and E–W (96° azimuth) directions (Figure 6). The anomalous sample from the lower part of PV1 (Figure 6, yellow symbols) has a **K1** direction perpendicular to the mean flow direction, suggesting higher velocity flows (e.g. Tarling and Hrouda 1993; Ellwood and Ledbetter 1977; Taira and Scholle 1979). This may be the result of a tsunami current flow; such a pattern is typical of shear and traction mode acting during deposition of the basal part of a tsunami deposit (Wassmer *et al.* 2010).

5.1. *Storm* versus *tsunami*

Additional evidence to support the probable tsunami origin of units PV1 and PV2 is their distance from the shoreline. To estimate the maximum inundation distance of extreme meteorological events (storms) on this section of the Pacific coast, we analysed historical storm and hurricane data for the period from 1949 to 2009 (NOAA (National Oceanic Atmospheric Administration) 2012). These data indicate that 29 of the 52 storms recorded during this period were hurricanes, of which only four were Category 4. Additional historical data indicate 14 tropical storms for the period from 1932 to 1934 (El Informador 1932, 1934). These records do not indicate the magnitude of the events, but they note the damage caused inland mainly by river floods as a result of heavy rain. In only one instance is damage to a coastal town (Puerto Vallarta, more than 250 km northwest) mentioned, although this may reflect the small population along the coast at that time.

Although winds up to 140 km hour^{-1} may have hit the Jalisco-Colima in 1959 during a Category 4 hurricane (or during the other three Category 4 events between 1949 and 2009), there are no reports that specifically describe wind or storm surge in sparsely populated areas such as PV. However, these events were likely associated with wave set-ups of several metres as a result of strong onshore winds. At PV though, while the site may only be 2 masl, it is around 275 m from the present shoreline, and about 200 m from the current estuary mouth, sufficiently landward to isolate it from most storm inundation (Figure 2c). Furthermore, the seaward sand dunes about 100 m from the coast exceed 7 masl, which did not prevent extensive flooding caused by the 1932 tsunami (Corona and Ramírez-Herrera 2012a) but are unlikely to have been over-topped by any historical storms. While the shoreline configuration may have changed over the past few hundred years, it seems reasonable to infer from the coastal geomorphology that a substantial sand barrier has been in place here for much of the Holocene. On balance, it seems most likely that both PV1 and PV2 relate to tsunami as opposed to storm inundation.

5.2. *Event chronologies*

The age of the PV events is based on a ^{210}Pb sequence and five ^{14}C dates. As discussed above, the CIC model ^{210}Pb chronology of the PV core yielded a date of CE1945 ± 13 at 10–11 cm for PV1. This age strongly supports that this deposit is associated with one of the June 1932 events. While ^{210}Pb data may have moderately low levels of activity, the two methods for determining the sediment age are consistent. The historical reconstruction and inundation model of Corona and Ramírez-Herrera (2012a) provides conclusive evidence that the PV site was only inundated by the 22 June 1932 tsunami and not the 3 June event (Figure 7). We therefore infer from both ^{210}Pb and historical data that unit PV1 was most likely laid down by the 22 June 1932 tsunami.

As discussed above, the two radiocarbon dates within the bottom sand unit of PV (Figure 4, Table 2: at 86–87.5 and 83.5–85 cm depth) overlap between 1256 and 1347 CE with the date from the clayey-silt unit between PV1 and PV2 (Figure 4, Table 2: 41–42.5 cm depth). Statistically, these could all be contemporaneous, although they are separated by PV2 and so it is reasonable to infer that the upper date is slightly younger. Both samples from within PV2 (Figure 4, Table 2: 66–67.5 cm depth) however are older than all three of the bracketing dates. We consider this to be the result of older carbon being introduced by tsunami inundation. If this interpretation is correct, then PV2 is closely dated to around 1300 CE, or

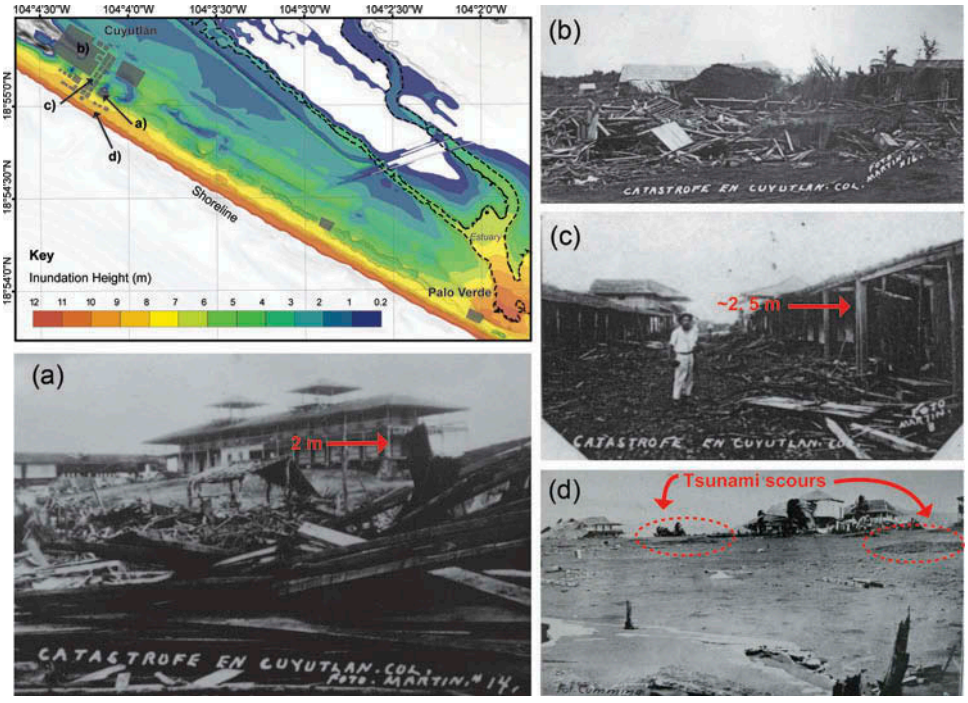

Figure 7. Inundation height distribution model of the 22 June 1932 tsunami; (a) Madrid Hotel; (b) Main Street; (c) railway station; main affected zone at Cuyutlán; (d) picture of tsunami scour, shown with red circles. Modified from Corona and Ramirez-Herrera (2012a). © The authors.

more correctly, sometime between 1256 and 1346 CE. It is worth nothing however that there are two alternative scenarios. First, it is possible that all the dates are reworked. However, the stratigraphic consistency and near-contemporaneity of three of the dates makes this an unlikely scenario. Second, because all of the dates are based on bulk organics, younger roots may have penetrated into older sediments, thus contaminating this deeper material. Again, this is unlikely given the near-contemporaneity of three of the samples and that all fine root material was removed before analysis.

Historical data indicate that on 16 November 1816, a tsunami reaching a height of 60 'codos' (i.e. equivalent to 25 m, or 34 m if this measurement refers to the 'codo real') flooded the coast of Cuyutlán, affecting the 'salinas' (salt pans for salt extraction) at Cuyutlán and El Real (southeast of Cuyutlán) (Galindo 1923; Marquina 1931; Guzmán-Nava 1954; Oseguera-Velázquez 1967; Ortoll 1988; Romero De Solís 1994; Sanmiguel 2001; Vázquez 2001; Suárez 2009). This is the oldest historically documented event predating the 22 June 1932 tsunami, and while it would seem reasonable to expect to find evidence for it at PV, the dating indicates that the previous event is considerably older. While this may seem surprising, it is worth noting that the geological evidence discussed above for PV1 (22 June 1932 tsunami) indicates that the unit has a sharp basal contact and it contains rip-up clasts. As such, this large event caused significant historically documented erosion (Chagué-Goff *et al.* 2012a), and this evidence helps to explain the notable hiatus between the young sediments of the 1932 tsunami and the underlying clayey-silt immediately beneath it that is some 500 years or more older. We therefore have most probably both a historically documented and a palaeotsunami at the same location.

5.3. *Multi-proxy data*

The tsunamigenic origin for an event should not be refuted because of the absence of one or more of the suite proxies that can be used to identify them, since they have never all been reported from a single location. Conversely, the presence of only a few proxies does not necessarily constitute conclusive evidence of tsunami origin (Goff *et al.* 2010a; Ramírez-Herrera *et al.* 2012, 2012a). Geological evidence for modern, historical, and palaeotsunamis has been widely described in the literature (e.g. Goff *et al.* 2001; Pinegina and Bourgeois 2001; Chagué-Goff *et al.* 2002; Gelfenbaum and Jaffe 2003; Moore *et al.* 2005; Kortekaas and Dawson 2007; Morton *et al.* 2007; Jankaew *et al.* 2008; Monecke *et al.* 2008, 2010b, 2011, 2012b). Similar geological evidence for the entire Mexican Pacific coast, however, is limited (Ramirez-Herrera *et al.* 2007, 2009,

2012), even though historical data on the occurrence of earthquakes and tsunamis extend back to the 1700s.

The results of this study complement previous geological work and help to create a more comprehensive record of past events along the Mexico's coast (Ramirez-Herrera *et al.* 2007, 2009; Ramírez-Herrera 2011, 2012). Multi-proxy data have proven to be an invaluable tool in determining the probable origin of the two sand deposits in this tropical environment. This work represents a growing trend in tsunami research where a much wider range of proxies are used to determine a tsunamigenic origin than the more conventional suite of sediment grain size and microfossils (diatoms and/or foraminifera) that have been used in the past. The latter proxies are still the most commonly used, especially in temperate environments where these basic indicators tend to be well preserved, but as more work is carried out in tropical regions, there is a need for a larger proxy toolkit to compensate for problems associated with intense physical and chemical weathering (Ramirez-Herrera *et al.* 2007; Goff *et al.* 2011a, 2011b, 2012, 2012b). The value of this approach in Mexico has been shown by our ability to identify the likely tsunamigenic origin of two sand units (Supplementary Document: Table 3). The correlation of sediment proxy information with historical, interview, numerical modelling, and post-tsunami survey data (Cumming 1933; Chagué-Goff *et al.* 2012a) has helped to further enhance our interpretation of the 22 June 1932 event. Our data represent a contribution to studies of onshore geological evidence of tsunamis in tropical coasts.

6. Conclusions

A wide range of multi-proxy data was collected from sediments in the Colima coastal area, from which depositional evidence for two probable tsunamis were identified in the PV estuary. These two events were probably associated with local tsunamigenic earthquakes. We link sand unit PV1 with the 22 June 1932 tsunami, which was most likely triggered by either a 'tsunami earthquake' or an earthquake-generated slump. Sand unit PV2 on the other hand relates to a probable palaeotsunami that occurred around 1300 CE (1284–1389 CE) which we suspect was associated with a similar seismic source.

This work shows that it is possible to identify both historical and palaeotsunamis in the tropical environment of Mexico's Pacific coast. The ability to identify and characterize such deposits, and differentiate them from past storms in this region, provides a unique opportunity to develop realistic estimates of the magnitude and frequency of past tsunamis. This information is vital for testing and constraining estimates of the tsunami hazard and for producing ground-truthed and realistic numerical inundation models. This, in turn, will greatly enhance our understanding of regional tsunami risk.

Acknowledgements

We are grateful to Ian Hutchinson for advice, help in the field, and reading the first draft of this manuscript. Violeta Rangel and P. Lacan assisted in the field, Cecila Caballero assisted with magnetic property analysis, and Eduardo A. Morales de la Garza assisted with grain size analysis. We thank Rocío Castillo for assisting with the historical archive data search. L. Bletcher worked with LOI and grain size analysis.

Funding

This research project was financially supported by a SEP-CONACYT grant assigned to Ramirez-Herrera [grant number CONACYT-129456]. J. Černý acknowledges the financial support by the Mexico Government student exchange programme – Secretaria de Relaciones Exteriores de México and the institutional support assigned as RVO: 67985831. Funding from the Australian Institute of Nuclear and Engineering (AINSE) grant 1ALNGRA for ^{210}Pb, ^{14}C dating, and ITRAX analyses is acknowledged.

Supplemental data

Supplemental data for this article can be accessed at http://dx.doi.org/10.1080/00206814.2014.951977.

References

Abe, K., Hakuno, M., Takeuchi, M., and Katada, T., 1986, Survey report on the tsunami of the Michoacan, México earthquake of September 19, 1985: Bulletin of the Earthquake Research Institute, v. 61, p. 475–481.

Appleby, P.G., 2001, Chronostratigraphic techniques in recent sediments, *in* Last, W.M., and Smol, J.P., eds., Tracking environmental change using lake sediments volume 1: basin analysis, coring and chronological techniques: Dordrecht, Kluwer Academic Publishers, p. 171–203.

Astiz, L., and Kanamori, H., 1984, An earthquake doublet in Ometepec, Guerrero, Mexico: Physics of the Earth and Planetary Interiors, v. 34, p. 24–45. doi:10.1016/0031-9201(84)90082-7

Atwater, B.F., Hedel, C.W., and Helley, E.J., 1977, Late quaternary depositional history, Holocene sea-level changes, and vertical crustal movement, Southern San Francisco Bay, California, U.S. Geological Survey Professional Paper 1014.

Atwater, B.F., and Hemphill-Haley, E., 1996, Preliminary estimates of tsunami recurrence intervals for great earthquakes of the past 3500 years at Northeastern Willapa Bay, Washington, US Geological Survey Open-File Report, 96-001.

Atwater, B.F., and Moore, A.L., 1992, A tsunami about 1000 years ago in Puget sound, Washington: Science, v. 258, p. 1614–1617. doi:10.1126/science.258.5088.1614

Atwater, B.F., Musumi-Rokkaku, S., Satake, K., Tsuji, Y., Ueda, K., and Yamaguchi, D.K., 2005, The orphan tsunami of 1700 – Japanese clues to a parent earthquake in North America, U. S. Geological Survey Professional Paper 1707, 133 p.

Baker, A., Allmendinger, R.W., Owen, L.A., and Rech, J.A., 2013, Permanent deformation caused by subduction earthquakes in northern Chile: Nature Geoscience, v. 6, p. 492–496. doi:10.1038/ngeo1789

Bronk Ramsey, C., 2009, Bayesian analysis of radiocarbon dates: Radiocarbon, v. 51, no. 1, p. 337–360.

Caballero, M., Peñalba, M.C., Martínez, M., Ortega-Guerrero, B., and Vázquez, L., 2005, A Holocene record from a former coastal lagoon in Bahía Kino, Gulf of California, Mexico: The Holocene, v. 15, p. 1236–1244. doi:10.1191/0959683605hl896rr

Carranza-Edwards, A., Kasper-Zubillaga, J.J., Rosales-Hoz, L., Morales-De La Garza, E.A., and Lozano-Santa Cruz, R., 2009, Beach sand composition and provenance in a sector of the southwestern Mexican Pacific: Revista Mexicana de Ciencias Geológicas, v. 26, no. 2, p. 433–447.

Chagué-Goff, C., 2010, Chemical signatures of palaeotsunamis: A forgotten proxy? Marine Geology, v. 271, p. 67–71. doi:10.1016/j.margeo.2010.01.010

Chagué-Goff, C., Andrew, A., Szczuciński, W., Goff, J., and Nishimura, Y., 2012a, Geochemical signatures up to the maximum inundation of the 2011 Tohoku-oki tsunami: Implications for the 869AD Jogan and other palaeotsunamis: Sedimentary Geology, v. 282, p. 65–77. doi:10.1016/j.sedgeo.2012.05.021

Chagué-Goff, C., Dawson, S., Goff, J.R., Zachariasen, J., Berryman, K.R., Garnett, D.L., Waldron, H.M., and Mildenhall, D.C., 2002, A tsunami (ca. 6300 years BP) and other Holocene environmental changes, northern Hawke's Bay, New Zealand: Sedimentary Geology, v. 150, p. 89–102. doi:10.1016/S0037-0738(01)00269-X

Chagué-Goff, C., Goff, J., Nichol, S.L., Dudley, W., Zawadzki, A., Bennett, J.W., Mooney, S.D., Fierro, D., Heijnis, H., Dominey-Howes, D., and Courtney, C., 2012b, Multi-proxy evidence for trans-Pacific tsunamis in the Hawai'ian Islands: Marine Geology, v. 299–302, p. 77–89. doi:10.1016/j.margeo.2011.12.010

Chagué-Goff, C., Schneider, J.-L., Goff, J.R., Dominey-Howes, D., and Strotz, L., 2011, Expanding the proxy toolkit to help identify past events – Lessons from the 2004 Indian Ocean Tsunami and the 2009 South Pacific Tsunami: Earth-Science Reviews, v. 107, p. 107–122. doi:10.1016/j.earscirev.2011.03.007

Cisternas, M., Atwater, B.F., Torrejón, F., Sawai, Y., Machuca, G., Lagos, M., Eipert, A., Youlton, C., Salgado, I., Kamataki, T., Shishikura, M., Rajendran, C.P., Malik, J.K., Rizal, Y., and Husni, M., 2005, Predecessors of the giant 1960 Chile earthquake: Nature, v. 437, p. 404–407. doi:10.1038/nature03943

Corona, N., and Ramírez-Herrera, M.T., 2012a, Mapping and historical reconstruction of the great Mexican 22 June 1932 tsunami: Natural Hazards and Earth System Sciences, v. 12, no. 5, 1337–1352. doi:10.5194/nhess-12-1337-2012

Corona, N., and Ramírez-Herrera, M.T., 2012b, Técnicas histórico-etnográficas en la reconstrucción y caracterización de tsunamis: El ejemplo del gran tsunami del 22 de junio de 1932, en las costas del Pacífico Mexicano: Revista de Geografía Norte Grande, v. 53, p. 102–122.

Cumming, J.L., 1933, Los terremotos de junio de 1932 en los estados de Colima y Jalisco: Universidad De México, v. 31–32, p. 68–104.

Curray, J.R., Emmel, F.J., and Crampton, P.J.S., 1969, Holocene history of a strand plain lagoonal coast, Nayarit, Mexico. *in* Lagunas costeras, Un simposio. Memorias Simposio Internacional, Lagunas costeras, UNAM-UNESCO, November 28–30, 1967, Mexico D.F., p. 63–100.

Cuven, S., Paris, R., Falvard, S., Miot-Noirault, E., Benbakkar, M., Schneider, J.-L., and Billy, I., 2013, High-resolution analysis of a tsunami deposit: Case-study from the 1755 Lisbon tsunami in southwestern Spain: Marine Geology, v. 337, p. 98–111. doi:10.1016/j.margeo.2013.02.002

Dearing, J.A., 1994, Environmental magnetic susceptibility—Using the MS2 Bartington System: Kenilworth, UK, Chi Publishing.

Dearing, J.A., Dann, R.J.L., Hay, K., Lees, J.A., Loveland, P.J., and O'Grady, K., 1996, Frequency-dependent susceptibility measurements of environmental materials: Geophysical Journal International, v. 124, p. 228–240. doi:10.1111/j.1365-246X.1996.tb06366.x

Dill, H.G., 2007, Grain morphology of heavy minerals from marine and continental placer deposits, with special reference to Fe–Ti oxides: Sedimentary Geology, v. 198, p. 1–27. doi:10.1016/j.sedgeo.2006.11.002

El Informador, 1932, Cuyutlán a punto de desaparecer bajo las aguas del Océano Pacífico, El Informador, p. 1–2, Junio 22, 1932.

Ellwood, B.B., and Ledbetter, M.T., 1977, Antarctic bottom water fluctuations in the Vema Channel: Effects of velocity changes on particle alignment and size: Earth and Planetary Science Letters, v. 35, p. 189–198. doi:10.1016/0012-821X(77)90121-2

Fink, D., Hotchkis, M., Hua, Q., Jacobsen, G., Smith, A.M., Zoppi, U., Child, D., Mifsud, C., Van Der Gaast, H., Williams, A., and Williams, M., 2004, The ANTARES AMS facility at ANSTO: Nuclear Instruments and Methods in Physics Research Section B: Beam Interactions with Materials and Atoms, v. 223–224, p. 109–115. doi:10.1016/j.nimb.2004.04.025

Folk, R.L., 1974, Petrology of sedimentary rocks: Austin, TX, Hemphill Publishing Co, 182 p.

Font, E., Nascimento, C., Omira, R., Baptista, M.A., and Silva, P. F., 2010, Identification of tsunami-induced deposits using numerical modeling and rock magnetism techniques: A study case of the 1755 Lisbon tsunami in Algarve, Portugal: Physics of the Earth and Planetary Interiors, v. 182, p. 187–198. doi:10.1016/j.pepi.2010.08.007

Font, E., Veiga-Pires, C., Pozo, M., Nave, S., Costas, S., Ruiz Muñoz, F., Abad, M., Simões, N., Duarte, S., and Rodríguez-Vidal, J., 2013, Benchmarks and sediment source(s) of the 1755 Lisbon tsunami deposit at Boca do Rio Estuary: Marine Geology, v. 343, p. 1–14. doi:10.1016/j.margeo.2013.06.008

Galindo, M., 1923, Elementos de geografía de Colima. Imprenta de "El Dragón", Colima, México.

Gelfenbaum, G., and Jaffe, B., 2003, Erosion and sedimentation from the 17 July 1998 Papua New Guinea tsunami: Pure and Applied Geophysics, v. 160, p. 1969–1999. doi:10.1007/s00024-003-2416-y

Goff, J., Chagué-Goff, C., Dominey-Howes, D., McAdoo, B., Cronin, S., Bonté-Grapetin, M., Nichol, S., Horrocks, M., Cisternas, M., Lamarche, G., Pelletier, B., Jaffe, B., and Dudley, W., 2011a, Palaeotsunamis in the Pacific Islands: Earth-Science Reviews, v. 107, p. 141–146. doi:10.1016/j.earscirev.2010.10.005

Goff, J., Chagué-Goff, C., and Nichol, S., 2001, Palaeotsunami deposits: A New Zealand perspective: Sedimentary Geology, v. 143, p. 1–6. doi:10.1016/S0037-0738(01)00121-X

Goff, J., Chagué-Goff, C., Nichol, S., Jaffe, B., and Dominey-Howes, D., 2012a, Progress in palaeotsunami research: Sedimentary Geology, v. 243–244, p. 70–88. doi:10.1016/j.sedgeo.2011.11.002

Goff, J., Lamarche, G., Pelletier, B., Chagué-Goff, C., and Strotz, L., 2011b, Predecessors to the 2009 South Pacific tsunami in the Wallis and Futuna archipelago: Earth-Science Reviews, v. 107, p. 91–106. doi:10.1016/j.earscirev.2010.11.003

Goff, J., Lane, E.M., and Arnold, J., 2009, The tsunami geomorphology of coastal dunes: Natural Hazards and Earth System Sciences, v. 9, p. 847–854. doi:10.5194/nhess-9-847-2009

Goff, J., McFadgen, B.G., Chague-Goff, C., and Nichol, S.L., 2012b, Palaeotsunamis and their influence on Polynesian settlement: The Holocene, v. 22, p. 1067–1069. doi:10.1177/0959683612437873

Goff, J., Nichol, S.L., and Kennedy, D., 2010a, Development of a palaeotsunami database for New Zealand: Natural Hazards, v. 54, p. 193–208. doi:10.1007/s11069-009-9461-5

Goff, J., Pearce, S., Nichol, S.L., Chagué-Goff, C., Horrocks, M., and Strotz, L., 2010b, Multi-proxy records of regionally-sourced tsunamis, New Zealand: Geomorphology, v. 118, p. 369–382. doi:10.1016/j.geomorph.2010.02.005

Goguitchaichvili, A., Ramírez-Herrera, M.T., Calvo-Rathert, M., Aguilar Reyes, B., Carrancho, Á., Caballero, C., Bautista, F., and Morales Contreras, J., 2013, Magnetic fingerprint of tsunami-induced deposits in the Ixtapa-Zihuatanejo area, Western Mexico: International Geology Review, v. 55, p. 1462–1470. doi:10.1080/00206814.2013.779781

Goto, G., Takahashi, J., and Fujino, S., 2012a, Variations in the 2004 Indian Ocean tsunami deposits thickness and their preservation potential, southwestern Thailand: Earth, Planets and Space, v. 64, p. 923–930. doi:10.5047/eps.2011.08.019

Goto, K., Chagué-Goff, C., Fujino, S., Goff, J., Jaffe, B., Nishimura, Y., Richmond, B., Sugawara, D., Szczuciński, W., Tappin, D.R., Witter, R.C., and Yulianto, E., 2011, New insights of tsunami hazard from the 2011 Tohoku-oki event: Marine Geology, v. 290, p. 46–50. doi:10.1016/j.margeo.2011.10.004

Goto, K., Chagué-Goff, C., Goff, J., and Jaffe, B.E., 2012b, The future of tsunami research following the 2011 Tohoku-oki event: Sedimentary Geology, v. 282, p. 1–13. doi:10.1016/j.sedgeo.2012.08.003

Goto, K., Hashimoto, K., Sugawara, D., Yanagisawa, H., and Abe, T., 2014, Spatial thickness variability of the 2011 Tohoku-oki tsunami deposits along the coastline of Sendai Bay: Marine Geology, http://dx.doi.org/10.1016/j.margeo.2013.12.015.

Guzmán-Nava, R., 1954, Geografía del estado de Colima: para uso de las escuelas primarias: Colima, Comisión Editora de El Nacional, v. 5, 135 p.

Harrison, J., Heijnis, H., and Caprarelli, G., 2003, Historical pollution variability from abandoned mine sites, Greater Blue Mountains World Heritage Area, New South Wales, Australia: Environmental Geology, v. 43, p. 680–687.

Hawkes, A.D., Bird, M., Cowie, S., Grundy-Warr, C., Horton, B. P., Shau Hwai, A.T., Law, L., Macgregor, C., Nott, J., Ong, J. E., Rigg, J., Robinson, R., Tan-Mullins, M., Sa, T.T., Yasin, Z., and Aik, L.W., 2007, Sediments deposited by the 2004 Indian Ocean Tsunami along the Malaysia-Thailand Peninsula: Marine Geology, v. 242, p. 169–190. doi:10.1016/j.margeo.2007.02.017

Heller, F., Shen, C.D., Beer, J., Liu, X.M., Liu, T.S., Bronger, A., Suter, M., and Bonani, G., 1993, Quantitative estimates of pedogenic ferromagnetic mineral formation in Chinese loess and palaeoclimatic implications: Earth and Planetary Science Letters, v. 114, p. 385–390, doi:10.1016/0012-821X(93)90038-B.

HTDB/WLD (Historical Tsunami Database for the World Ocean) 2013, http://tsun.sscc.ru/nh/tsunami.php, last access: 10 April 2013.

Hustedt, F., 1957, Die Diatomeenflora des Fluss-Systems der Weserim Gebiet der Hansestadt Bremen: Bremen, Abhandlungen Naturwissenschaftlicher Verein, 34.

Hutchinson, I., Clague, J.C., and Mathewes, R.W., 1997, Reconstructing the tsunami record on an emerging coast: A case study of Kanim Lake, Vancouver Island, British Columbia, Canada: Journal of Coastal Research, v. 13, p. 545–553.

Informador, E., 1934, Están en ruinas los pueblos que fueron azotados por el ciclón del mes pasado. El Informador, p. 13, 4 de Noviembre, 1934.

Jankaew, K., Atwater, B.F., Sawai, Y., Choowong, M., Charoentitirat, T., Martin, M.E., and Prendergast, A., 2008, Medieval forewarning of the 2004 Indian Ocean tsunami in Thailand: Nature, v. 455, p. 1228–1231. doi:10.1038/nature07373

Jelinek, V., 1981, Characterization of the magnetic fabric of rocks: Tectonophysics, v. 79, p. T63–T67. doi:10.1016/0040-1951(81)90110-4

Kamatani, A., 1982, Dissolution rates of silica from diatoms decomposing at various temperatures: Marine Biology, v. 68, p. 91–96. doi:10.1007/BF00393146

Kench, P.S., McLean, R.F., Brander, R.F., Nichol, S.L., Smithers, S.G., Ford, M.R., Parnell, K.E., and Aslam, M., 2006, Geological effects of tsunami on mid-ocean atoll islands: The Maldives before and after the Sumatran tsunami: Geology, v. 34, p. 177–180. doi:10.1130/G21907.1

Kench, P.S., Nichol, S.L., Smithers, S.G., McLean, R.F., and Brander, R.W., 2008, Tsunami as agents of geomorphic change in mid-ocean reef islands: Geomorphology, v. 95, p. 361–383. doi:10.1016/j.geomorph.2007.06.012

Kortekaas, S., and Dawson, A.G., 2007, Distinguishing tsunami and storm deposits: An example from Martinhal, SW Portugal: Sedimentary Geology, v. 200, p. 208–221. doi:10.1016/j.sedgeo.2007.01.004

Lancin, M., and Carranza, A., 1976, Estudio geomorfológico de la bahía y la playa de Santiago en Manzanillo Colima: Revista Del Instituto De Geología UNAM, v. 2, p. 43–65.

Liu, P.L.F., Lynett, P., Fernando, P., Jaffe, H., Fritz, B., Higman, H., Morton, B., Goff, J., and Synolakis, C., 2005, Observations by the International Tsunami Survey Team in Sri Lanka: Science, v. 308, p. 1595. doi:10.1126/science.1110730

Maher, B.A., Thompson, R., and Zhou, L.P., 1994, Spatial and temporal reconstructions of changes in the Asian palaeomonsoon: A new mineral magnetic approach: Earth and Planetary Science Letters, v. 125, p. 461–471. doi:10.1016/0012-821X(94)90232-1

Marquina, I., 1931, Estudio comparativo entre los principales edificios prehispánicos en México: México, Impr. Mundial, 14 p.

Monecke, K., Finger, W., Klarer, D., Kongko, W., McAdoo, B. G., Moore, A.L., and Sudrajat, S.U., 2008, A 1,000-year sediment record of tsunami recurrence in northern Sumatra: Nature, v. 455, p. 1232–1234. doi:10.1038/nature07374

Moore, A., Gelfenbaum, G., and Triyono, R., 2005, Sedimentary deposits of the 26 December 2004 tsunami on the northwest coast of Aceh, Indonesia: Earth Planets Space, v. 58, p. 253–258.

Moore, A., Goff, J., McAdoo, B., Fritz, H., Gusman, A., Kalligeris, N., Kalsum, K., Susanto, A., Suteja, D., and Synolakis, C., 2011, Sedimentary deposits from the 17 July 2006 Western Java Tsunami, Indonesia: Use of grain size analyses to assess tsunami flow depth, speed, and traction carpet characteristics: Pure and Applied Geophysics, v. 168, p. 1951–1961. doi:10.1007/s00024-011-0280-8.

Morton, R.A., Gelfenbaum, G., and Jaffe, B.E., 2007, Physical criteria for distinguishing sandy tsunami and storm deposits

using modern examples: Sedimentary Geology, v. 200, p. 184–207. doi:10.1016/j.sedgeo.2007.01.003

Nagata, T., Rock Magnetism (second edition): Tokyo, Maruzen Company, 350 p.

Nanayama, F., Satake, K., Furukawa, R., Shimokawa, K., Atwater, B.F., Shigeno, K., and Yamaki, S., 2003, Unusually large earthquakes inferred from tsunami deposits along the Kuril trench: Nature, v. 424, p. 660–663. doi:10.1038/nature01864

Nelson, A.R., Kelsey, H.M., and Witter, R.C., 2006, Great earthquakes of variable magnitude at the Cascadia subduction zone: Quaternary Research, v. 65, p. 354–365. doi:10.1016/j.yqres.2006.02.009

NGDC (National Geophysical Data Center – National Oceanic and Atmospheric Administration). 2013 NOAA/WTC Tsunami Event Database 2013 [cited 2013 April].

NOAA (National Oceanic Atmospheric Administration) 2012, Historical hurricanes tracks. http://www.csc.noaa.gov/hurricanes/# (accessed February 2013).

Okal, E.A., and Borrero, J.C., 2011, The tsunami earthquake of 1932 June 22 in Manzanillo, México: Seismological study and tsunami simulations: Geophysical Journal International, v. 187, no. 3, p. 1–17. doi:10.1111/j.1365-246X.2011.05199.x

Ortlieb, L., 1986. Nectonique et variations du niveau marin au Quaternaire dans la region du Golfe de Californie, Mexique Doctorat d'Etat Thesis, Universite d'Aix -_Marseille II, France, 2 vols.

Ortoll, S., 1988, Colima: Textos de su historia. Colección Historia Regional de México: México D.F., Editorial Mora, 374.

Oseguera-Velázquez, J.O., 1967, Colima en panorama: Monografía histórica, geográfica, política y sociológica: Colima, México, Impr. Al libro mayor, 392.

Papadopoulos, G.A., and Imamura, F., 2001, A proposal for a new tsunami intensity scale. ITS 2001 Proceedings, session 5-1, p. 569–577, Seattle.

Paris, R., Fournier, J., Poizot, E., Etienne, S., Morin, J., Lavigne, F., and Wassmer, P., 2010, Boulder and fine sediment transport and deposition by the 2004 tsunami in Lhok Nga (western Banda Aceh, Sumatra, Indonesia): A Coupled Offshore–Onshore Model, Marine Geology, v. 268, p. 43–54.

Paris, R., Lavigne, F., Wassmer, P., and Sartohadi, J., 2007, Coastal sedimentation associated with the December 26, 2004 tsunami in Lhok Nga, west Banda Aceh (Sumatra, Indonesia): Marine Geology, v. 238, p. 93–106. doi:10.1016/j.margeo.2006.12.009

Pinegina, T.K., and Bourgeois, J., 2001, Historical and paleo-tsunami deposits on Kamchatka, Russia: Long-term chronologies and long-distance correlations: Natural Hazards and Earth System Sciences, v. 1, p. 177–185. doi:10.5194/nhess-1-177-2001

Ramírez-Herrera, M.T., 2011, Evidencias ambientales de cambios de nivel de la costa del Pacífico de México: Terremotos y tsunamis: Revista de Geografía Norte Grande, v. 49, p. 99–124. doi:10.4067/S0718-34022011000200007

Ramírez-Herrera, M.T., Cundy, A., and Kostoglodov, V., 2005, Evidence of prehistoric earthquakes and tsunamis during the last 5000 years along the Guerrero Seismic Gap, Mexico: Proceedings of the XV CNIS Mexican Society of Seismic Engineering, v. I-07, p. 1–17.

Ramirez-Herrera, M.T., Cundy, A., Kostoglodov, V., Carranza-Edwards, A., Morales, E., and Metcalfe, S., 2007, Sedimentary record of late Holocene relative sea-level change and tectonic deformation from the Guerrero Seismic Gap, Mexican Pacific Coast: The Holocene, v. 17, p. 1211–1220. doi:10.1177/0959683607085127

Ramírez-Herrera, M.T., Cundy, A., Kostoglodov, V., and Ortiz, M., 2009, Late Holocene tectonic land-level changes and tsunamis at Mitla lagoon, Guerrero, México: Geofísica Internacional, v. 48, p. 195–209.

Ramírez-Herrera, M.T., Lagos, M., Hutchinson, I., Kostoglodov, V., Machain, M.L., Caballero, M., Goguitchaichvili, A., Aguilar, B., Chagué-Goff, C., Goff, J., Ruiz-Fernández, A.-C., Ortiz, M., Nava, H., Bautista, F., Lopez, G.I., and Quintana, P., 2012, Extreme wave deposits on the Pacific coast of Mexico: Tsunamis or storms? – A multi-proxy approach: Geomorphology, v. 139–140, p. 360–371. doi:10.1016/j.geomorph.2011.11.002

Rees, A.I., and Woodall, W.A., 1975, The magnetic fabric of some laboratory-deposited sediments: Earth and Planetary Science Letters, v. 25, p. 121–130. doi:10.1016/0012-821X(75)90188-0

Reimer, P.J., Bard, E., Bayliss, A., Beck, J.W., Blackwell, P.G., Bronk Ramsey, C., Grootes, P.M., Guilderson, T.P., Haflidason, H., Hajdas, I., HattŽ, C., Heaton, T.J., Hoffmann, D.L., Hogg, A.G., Hughen, K.A., Kaiser, K.F., Kromer, B., Manning, S.W., Niu, M., Reimer, R.W., Richards, D.A., Scott, E.M., Southon, J.R., Staff, R.A., Turney, C.S.M., and Van Der Plicht, J., 2013, IntCal13 and Marine13 radiocarbon age calibration curves 0–50,000 years cal BP: Radiocarbon, v. 55, no. 4, p. 1869–1887. doi:10.2458/azu_js_rc.55.16947.

Romero De Solís, J.M., 1994, Breve historia de Colima: México, D.F, Fondo de cultura económica.

Rothwell, R.G., Hoogakker, B., Thomson, J., Croudace, I.W., and Frenz, M., 2006, Turbidite emplacement on the southern Balearic Abyssal Plain (western Mediterranean Sea) during Marine Isotope Stages 1–3: An application of ITRAX XRF scanning of sediment cores to lithostratigraphic analysis, *in* Rothwell, R.G., ed., New techniques in sediment core analysis: Geological Society of London, Special Publications, v. 267, p. 79–98.

Sánchez, A.J., and Farreras, S.F., 1993, Catálogo de tsunamis (maremotos) en la costa occidental de México: United States, Geological Survey, World Data Center A for solid Earth Geophysics Publication, Vol. SE-50: 94 p.

Sanmiguel, R.H., 2001, Estaciones ferroviarias de la ruta Guadalajara-Manzanillo: Colima, México, Gobierno del Estado de Colima, Secretaría de Cultura.

Sawai, Y., Jankaew, K., Martin, M.E., Prendergast, A., Choowong, M., and Charoentitirat, T., 2009, Diatom assemblages in tsunami deposits associated with the 2004 Indian Ocean tsunami at Phra Thong Island, Thailand: Marine Micropaleontology, v. 73, p. 70–79. doi:10.1016/j.marmicro.2009.07.003

Schneider, J.-L., Chagué-Goff, C., Bouchez, J.-L., Goff, J., Sugawara, D., Goto, K., Jaffe, B., Richmond, B., and Szczuciński, W., 2014, Using magnetic fabric to reconstruct the dynamics of tsunami deposition on the Sendai Plain, Japan – The 2011 Tohoku-oki tsunami: Marine Geology. doi:10.1016/j.margeo.2014.06.010, in press.

Singh, S.K., Havskov, J., and Astiz, L., 1981, Seismic gaps and recurrence periods of large earthquakes along the Mexican subduction zone: Bulletin of the Seismology Society of America, v. 71, p. 827–843.

Singh, S.K., Pacheco, J., and Shapiro, N.M., 1998, The earthquake of 16 November, 1925 (Ms = 7.0) and the Reported tsunami in Zihuatenejo, Mexico: Instituto De Geofísica, UNAM, v. 37, p. 49–52.

Singh, S.K., Ponce, L., and Nishenko, S.P., 1985, The great Jalisco, Mexico, earthquakes of 1932: subduction of the

Rivera plate: Bulletin of the Seismological Society of America, v. 75, no. 5, p. 1301–1313.
Sirkin, L., 1985, Late quaternary stratigraphy and environments of the west Mexican coastal plain: Palynology, v. 9, p. 3–25. doi:10.1080/01916122.1985.9989285
Stuiver, M., and Polach, H., 1977, Reporting of ^{14}C data: Radiocarbon, v. 19, p. 355–363.
Suárez, C.M., 2009, Métrica en Arquitectura (1a): México, Universidad Iberoamericana.
Suarez, G., and Albini, P., 2009, Evidence for Great Tsunamigenic Earthquakes (M 8.6) along the Mexican Subduction Zone: Bulletin of the Seismological Society of America, v. 99, p. 892–896. doi:10.1785/0120080201
Szczuciński, W., Chaimanee, N., Niedzielski, P., Rachlewicz, G., Saisuttichai, D., Tepsuwan, T., Lorenc, S., and Siepak, J., 2006, Environmental and geological impacts of the 26 December 2004 Tsunami in coastal zone of Thailand – Overview of short and long-term effects: Polish Journal of Environmental Studies, v. 15, no. 5, p. 793–810.
Szczuciński, W., Kokociński, M., Rzeszewski, M., Chagué-Goff, C., Cachão, M., Goto, K., and Sugawara, D., 2012, Sediment sources and sedimentation processes of 2011 Tohoku-oki tsunami deposits on the Sendai Plain, Japan – Insights from diatoms, nannoliths and grain size distribution: Sedimentary Geology, v. 282, p. 40–56. doi:10.1016/j.sedgeo.2012.07.019
Taira, A., 1989, Magnetic fabrics and depositional processes, *in* Taira, A., and Masuda, F., eds., Sedimentary facies in the active plate margin: Tokyo, Terra Sci Publishing, p. 43–77.
Taira, A., and Scholle, P.A., 1979, Deposition of resedimented sandstone beds in the Pico Formation, Ventura Basin, California, as interpreted from magnetic fabric measurements: Geological Society of America Bulletin, v. 90, p. 952–962. doi:10.1130/0016-7606(1979)90<952:DORSBI>2.0.CO;2
Tarling, D.H., and Hrouda, F., 1993, The magnetic anisotropy of rocks: London, Chapman and Hall.
Tuttle, M.P., Ruffman, A., Anderson, T., and Jeter, H., 2004, Distinguishing tsunami from storm deposits in Eastern North America: The 1929 Grand Banks Tsunami versus the 1991 Halloween Storm: Seismological Research Letters, v. 75, no. 1, p. 117–131. doi:10.1785/gssrl.75.1.117
Valdivia, O.L., Castillo-Aja, M.R., and Trejo, E.M., 2012, Tsunamis en Jalisco: Geocalli, Cuadernos De Geografía, Universidad de Guadalajara. Año v. 13, no. 25, p. 103.
Vázquez, J.L., 2001, Los terremotos de 1932: México, Gobierno del Estado De Colima, Secretaría de Cultura.
Voorhies, B., 2004, Coastal Collectors in the Holocene: The Chantuto People of Southwest Mexico: Gainesville, University Press of Florida.
Walker, W.G., Davidson, G.R., Lange, T., and Wren, D., 2007, Accurate lacustrine and wetland sediment accumulation rates determined from ^{14}C activity of bulk sediment fractions: Radiocarbon, v. 49, p. 983–992.
Wassmer, P., Schneider, J.-L., Fonfrège, A.-V., Lavigne, F., Paris, R., and Gomez, C., 2010, Use of anisotropy of magnetic susceptibility (AMS) in the study of tsunami deposits: Application to the 2004 deposits on the eastern coast of Banda Aceh, North Sumatra, Indonesia: Marine Geology, v. 275, p. 255–272. doi:10.1016/j.margeo.2010.06.007
Yawsangratt, S., Szczuciński, W., Chaimanee, N., Chatprasert, S., Majewski, W., and Lorenc, S., 2012, Evidence of probable paleotsunami deposits on Kho Khao Island, Phang Nga Province, Thailand: Natural Hazards, v. 63, p. 151–163. doi:10.1007/s11069-011-9729-4